processes

MDPI

*Article*

# Economic and Technical Assessing the Hybridization of Solar Combined Cycle System with Fossil Fuel and Rock Bed Thermal Energy Storage in Neom City

**Abdulrazzak Akroot [1] and Abdullah Sultan Al Shammre [2,*]**

[1] Mechanical Engineering Department, Faculty of Engineering, Karabük University, 78050 Karabük, Turkey; abdulrazzakakroot@karabuk.edu.tr
[2] Economics Department, College of Business Administration, King Faisal University, Al-Ahsa 31982, Saudi Arabia
* Correspondence: ashammre@kfu.edu.sa

**Abstract:** Rising energy demands, the depletion of fossil fuels, and their environmental impact necessitate a shift towards sustainable power generation. Concentrating solar power (CSP) offers a promising solution. This study examines a hybridization of a combined cycle power plant (CCPP) based on solar energy with fossil fuel and energy storage in rock layers to increase Saudi Arabia's electricity production from renewable energy. The fuel is used to keep the temperature at the inlet of the gas turbine at 1000 °C, ensuring the power produced by the Rankine cycle remains constant. During the summer, the sun is the main source of power generation, whereas in the winter, reliance on fuel increases significantly. The Brayton cycle operates for 10 h during peak solar radiation periods, storing exhaust heat in rock beds. For the remaining 14 h of the day, this stored heat is discharged to operate the Rankine steam cycle. Simulations and optimizations are performed, and the system is evaluated using a comprehensive 4E analysis (energy, exergy, exergoconomic, and environmental) alongside a sustainability assessment. A parametric evaluation examines the effect of key factors on system performance. The rock bed storage system compensates for solar intermittency, enabling power generation even without sunlight. The study reveals that the system generated 12.334 MW in June, achieving an energy efficiency of 37% and an exergy efficiency of 40.35%. The average electricity cost during this period was 0.0303 USD/kWh, and the carbon footprint was 0.108 kg $CO_2$/kWh. In contrast, during January, the system produced 13.276 MW with an energy efficiency of 37.91% and an exergy efficiency of 44.16%. The average electricity cost in January was 0.045 USD/kWh, and the carbon footprint was 0.1 kg $CO_2$/kWh. Interestingly, solar energy played a significant role: it contributed 81.42% of the heat in June, while in January, it accounted for 46.77%. The reduced electricity costs during June are primarily attributed to the abundant sunshine, which significantly powered the system.

**Keywords:** combined cycle power plant (CCPP); concentrating solar power (CSP); exergoconomic; rock bed storage system (RBES); Neom City



**Citation:** Akroot, A.; Al Shammre, A.S. Economic and Technical Assessing the Hybridization of Solar Combined Cycle System with Fossil Fuel and Rock Bed Thermal Energy Storage in Neom City. *Processes* **2024**, *12*, 1433. https://doi.org/10.3390/pr12071433

Academic Editors: Alvaro Ochoa, Gustavo De Novaes Pires Leite and José Ângelo Peixoto Da Costa

Received: 11 June 2024
Revised: 3 July 2024
Accepted: 5 July 2024
Published: 9 July 2024



## 1. Introduction

Solar thermal power stations that use thermal energy storage (TES) are an alternative to traditional fossil fuels [1]. Solar thermal power stations use the sun's limitless energy supplies rather than the limited fossil fuels used by traditional power plants, which cause pollution. These plants play a vital role in combating climate change and reducing greenhouse gas emissions by converting solar heat into electricity. Incorporating TES into solar thermal power plants is a novel approach [2–4]. The system efficiently uses solar energy to generate electricity and includes a storage system to provide a consistent power supply, even under low sunshine conditions [5].

Many research projects have focused on thermal energy storage devices and how they might be integrated into power plant operations. Soprani et al. [6] focused on a high-temperature TES prototype using diabase rocks and air for heat transfer, aiming to store heat at 600 °C with 450 kWhth capacity. They analyzed the system's temperature and flow patterns during charging and discharging, looking into efficiency and heat retention metrics. Desai et al. [7] investigated a new, cost-effective concentrated solar power system employing a micro-structured polymer foil for solar concentration. Their study compared three thermal energy storage options, emphasizing the optimal design for cogeneration systems in terms of cost and efficiency. Marongiu et al. [8] offered insights through a 2-D numerical model of a 450 kWhth rock bed, considering the temperature-dependency of air and rocks to evaluate design factors like the rock size and type on the system efficiency. Zanganeh et al. [9] detailed a 6.5 MWhth air-and-rock thermal storage unit, analyzing a numerical model that aligns closely with experimental data for an accurate heat transfer representation. Nahhas et al. [10] assessed basalt rocks for thermal storage, finding them suitable up to 700 °C due to their thermal and mechanical properties. Kocak and Paksoy [11] tested an affordable and eco-friendly material for thermal storage in low-temperature industrial solar applications. Sharma et al. [12] evaluated packed-bed TES systems with different materials, identifying hybrid particles as the most effective storage medium. Heller and Gauche [13] proposed a rock bed heat transfer model for storing and transmitting energy to steam cycles, using simulations to examine its influence on power plant economics. Abdulla and Reddy [14] modeled the heat transfer in a molten salt-packed-bed system for CSP plants, identifying key parameters for efficient energy discharge. Öztürk et al. [15] introduced a combined gas and steam turbine system with a rock bed TES for diversified heating and power applications, conducting extensive analyses on performance and efficiency under variable conditions. Fernández et al. [16] analyzed operation strategies for packed bed TES systems to enhance efficiency and thermal storage behavior. Pelay et al. [17] assessed the TES systems in concentrated solar power (CSP) plants. They discussed the global status of CSP, various high-temperature TES technologies (200–1000 °C), thermochemical storage, and new integration strategies for TES in CSP. Freeman et al. [18] evaluated the TES solutions for domestic solar combined heat and power systems using ORC engines and solar–thermal collectors. The study discussed how TES enhances system efficiency, aligns with user demands, and reduces costs, especially under variable solar conditions. Çam et al. [19] assessed a solar-assisted heat pump-integrated latent heat TES system for variable-temperature heating. The authors investigated using phase change materials (PCMs) with different characteristics to improve solar energy intermittency and energy efficiency. According to the research, the best PCM settings may save operating expenses considerably, boost heat pump performance by 35% to 80%, and provide a payback time of around 13 years in Izmir. Khamlich et al. [20] conducted a techno-economic analysis of a 100 MWe CSP plant with various TES configurations, assessing their integration into a spot market. Al-Nimr et al. [21] found that a CPV/T solar power system with ORC, a geothermal condenser, and energy storage can achieve up to 22% efficiency in November. Shakouri et al. [22] analyzed a multigeneration system integrating conventional and renewable energy sources, achieving enhanced efficiency and sustainability with significant reductions in fuel use and CO2 emissions. Kuterbekov et al. [23] assessed a hybrid power system utilizing solar and biomass energy to produce electricity, heat, and hydrogen, demonstrating cost efficiencies and exergy improvements through the innovative use of heat exchangers and polymer membrane electrolyzers, with the system's performance analyzed using the ESS tool (https://fchartsoftware.com/ees/). Zhang et al. [24] analyzed energy and exergy losses during the startup of PTC solar power plants using molten salt. They demonstrated that a molten salt anti-freezing solution can reduce startup energy consumption. Wang et al. [25] proposed a hybrid hydrogen production and gas–solar power system integrating a solar tower, a gas–steam turbine, and an organic Rankine cycle, achieving 103.9 MW power and 41.3% efficiency with stable operations and identifying areas for performance enhancement in exergy losses. Table 1 provides a summary of the

reviewed research on thermal energy storage devices and their potential integration into power plant operations.

**Table 1.** Summary of reviewed research on thermal energy storage devices and their potential integration into power plant operations.

| Author(s) | Focus | Key Findings |
| --- | --- | --- |
| Soprani et al. [6] | High-temperature TES prototype using diabase rocks and air for heat transfer | Analyzed temperature and flow patterns during charging and discharging for a system with 450 kWh capacity and operated at 600 °C |
| Desai et al. [7] | Cost-effective concentrated solar power system with micro-structured polymer foil | Compared three thermal energy storage options, optimal design for cogeneration systems |
| Marongiu et al. [8] | 2-D numerical model of a rock bed considering temperature-dependency of air and rocks | Evaluated design factors like rock size and type on system efficiency |
| Sharma et al. [12] | Packed-bed TES systems with different materials, identifying hybrid particles as the most effective | Identified hybrid particles as the most effective storage medium |
| Heller et al. [13] | Rock bed heat transfer model for energy storage and transmission to steam cycles | Simulations examined the influence on power plant economics |
| Abdulla et al. [14] | Heat transfer in molten salt-packed-bed system for CSP plants | Identified key parameters for efficient energy discharge |
| Öztürk et al. [15] | Combined gas and steam turbine system with rock bed TES for diversified heating and power applications | Conducted extensive analyses on performance and efficiency under variable conditions |
| Fernández et al. [16] | Operation strategies for packed bed TES systems to enhance efficiency and thermal storage behavior | Enhanced efficiency and thermal storage behavior |
| Pelay et al. [17] | TES systems in CSP plants, discussing high-temperature TES technologies and integration strategies | Discussed global status of CSP, various high-temperature TES technologies, and new integration strategies |
| Freeman et al. [18] | TES solutions for domestic solar combined heat and power systems using ORC engines and solar–thermal collectors | TES enhances system efficiency, aligns with user demands, and reduces costs |
| Çam et al. [19] | Solar-assisted heat pump-integrated latent heat TES system for variable-temperature heating using PCMs | Investigated PCMs to improve solar energy intermittency and energy efficiency |
| Khamlich et al. [20] | Techno-economic analysis of a 100 MWe CSP plant with various TES configurations | Assessed TES integration into spot market for economic performance |
| Shakouri et al. [22] | Multigeneration system integrating conventional and renewable energy sources | Enhanced efficiency and sustainability with significant reductions in fuel use and CO2 emissions |
| Zhang et al. [24] | Energy and exergy losses during the startup of PTC solar power plants using molten salt | Molten salt anti-freezing solution reduces startup energy consumption |
| Wang et al. [25] | Hybrid hydrogen production and gas-solar power system integrating solar tower, gas-steam turbine, and ORC | Achieved 103.9 MW power and 41.3% efficiency with stable operations |

This work presents a unique study that introduces a 4E analysis on a novel hybridization of a combined cycle based on solar energy with fossil fuels, featuring rock bed energy storage for reliable power supply during low sunlight. The research evaluates the plant's exergy efficiency, investment, and operational costs, focusing on how varying parameters influence the overall efficiency and cost-effectiveness, marking a distinct approach to analyzing solar-powered combined cycle systems.

## 2. System Description

The newly developed combined cycle power plant (CCPP) features a primary solar Brayton cycle (SBC), a secondary Rankine cycle (RC), and rock bed thermal energy storage (RBES). This research focused on the Neom region in Saudi Arabia. Figure 1 illustrates the CCPP system, which utilizes both solar and fuel energy. The SBC includes an air compressor, heliostats, solar receivers, a combustion chamber, and a gas turbine. The air compressor increases air pressure to 1469 kPa, which is then heated by a solar central receiver. The combustion chamber adjusts for solar light variations, maintaining the gas turbine's inlet temperature at 1000 °C using a small amount of $CH_4$ fuel for enhanced efficiency. Exhaust gases from the SBC pass through the RBES, storing energy during the day and enabling the RC to generate power at night without solar radiation. The RC uses hot exhaust gases from the GT stored in the RBES and benefits from the hot air produced by the RBES. The SBC operates for 10 h during peak solar radiation, storing hot exhaust in rocks. The remaining 14 h are used to run the Rankine steam cycle, with the system generating power from the SBC for 10 h and from the RC for 14 h. The temperature profile through the boiler is illustrated in Figure 2.

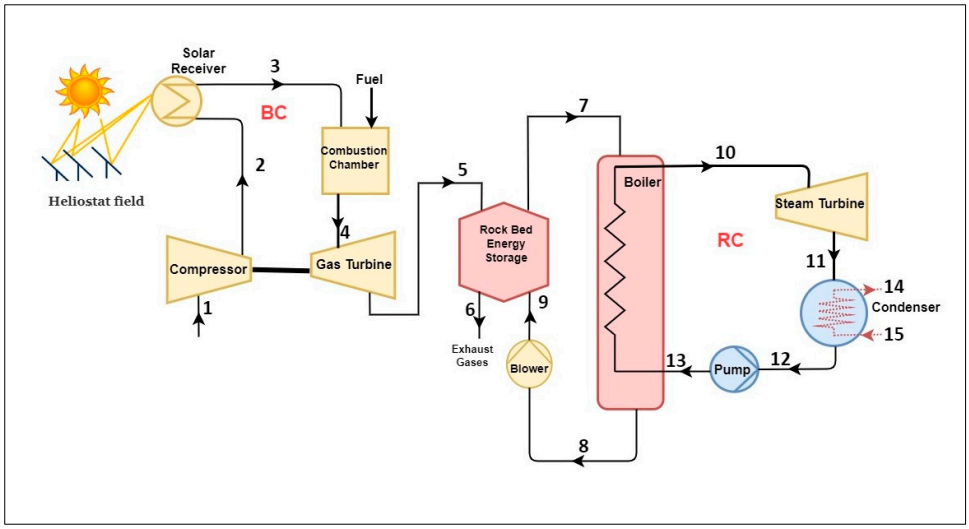


**Figure 1.** Combined cycle power plant (CCPP) schematic diagram.

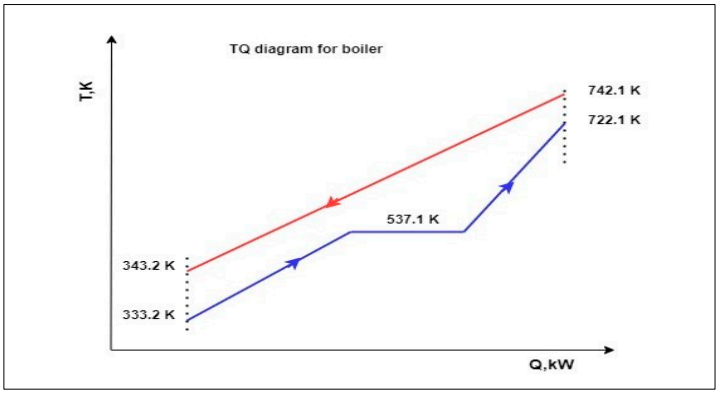


**Figure 2.** Temperature profile in the boiler.

The simulation in this work utilized Engineering Equation Solver (EES) software (https://fchartsoftware.com/ees/) for modeling and analysis, which calculates thermodynamic properties such as temperature, exergy, pressure, and entropy. The thermodynamic, exergoeconomic, and environmental studies are conducted with the following basic assumptions:

- The reference state pressure ($P_o$) is 1 bar, and the reference state temperature ($T_o$) is 25 °C.
- There is no change to either the kinetic or potential energy.
- The system is in a steady-state condition.
- The fuel is pure methane ($CH_4$).
- The sun's surface temperature is 6000 K.
- The turbines, pump, and compressor operate adiabatically.

The designed system involves individual thermodynamic modeling of each component. Equations specific to mass, energy, exergy, and exergoeconomic analyses are used, with detailed operational and technical parameters provided in Table 2.

**Table 2.** Operation conditions employed in the designed system.

| Component | Parameter | Value |
|---|---|---|
| AC | Compression ratio | 14.5 |
| | Ambient temperature | 33.65 °C |
| | Ambient pressure | 101.3 kPa |
| | Air flow rate | 52 kg/s |
| | Isentropic efficiency | 84% |
| Heliostats field | Area | 53,935 $m^2$ |
| | DNI | 8.02 (kW-h/$m^2$/day) |
| | Location | Neom, Saudi Arabia |
| | Latitude | 28.0064° |
| | Longitude | 35.2025° |
| GT | Inlet temperature | 1000 °C |
| | Isentropic efficiency | 85% |
| RBES | Time of charge | 10 h |
| | Time of discharge | 14 h |
| ST | Inlet pressure | 5000 kPa |
| | Isentropic efficiency | 80% |
| Pump | Isentropic efficiency | 90% |
| Condenser | Condenser temperature | 60 °C |

## 3. Thermodynamic Analysis

The system's mass balance equation is expressed as

$$\sum \dot{m}_{in} = \sum \dot{m}_{out} \quad (1)$$

The following equation represents the system's overall energy balance [26]:

$$\dot{Q}_{in} + \dot{W}_{in} + \sum \dot{m}_{in} h_{in} = \dot{Q}_{out} + \dot{W}_{out} + \sum \dot{m}_{out} h_{out} \quad (2)$$

The system's exergy balance equation may be written as follows: [27,28]:

$$\sum (\dot{m}e)_{in} + \dot{E}_{in,W} + \dot{E}_{in,Q} = \sum (\dot{m}e)_{out} + \dot{E}_{out,W} + \dot{E}_{out,Q} \quad (3)$$

$$\dot{E}^{Q} = \dot{Q}\left(1 - \frac{T_0}{T}\right) \quad (4)$$

$$\dot{m}_{in}\, S_{in} + \left(\frac{\dot{Q}}{T}\right) + \dot{S}_{gen} = \dot{m}_{out}\, S_{out} \quad (5)$$

The heat transfer rate by the solar receiver is determined using the following equations:

$$\dot{Q}_{Solar} = \dot{Q}_h - \dot{Q}_{rec,loss} \quad (6)$$

$$\dot{Q}_{Solar} = \dot{m}_3 h_3 - \dot{m}_2 h_2 = \dot{m}_3 c_{p,3} T_3 - \dot{m}_2 c_{p,2} T_2 \quad (7)$$

The following equations are used to compute the rate of heat transfer in the heliostat field and the rate of heat loss in the receiver [29]:

$$\dot{Q}_{rec,loss} = \dot{Q}_c + \dot{Q}_r = A_r \times \left[ h_c \times (T_r - T_0) + \sigma \times \varepsilon \times \left( T_r^4 - T_0^4 \right) \right] \quad (8)$$

$$\dot{Q}_h = A_h \times N \times I \times \eta_h \quad (9)$$

The convective heat transfer coefficient of air ($h_c$) can be calculated using the following formula, with units in $W/m^2K$ [15]:

$$h_c = 10.45 - V + 10\sqrt{V} \quad (10)$$

The SBC's outlet temperature and power consumption of the compressor are determined using the following equations [30]:

$$T_{out} = T_{in} \left( 1 + \frac{1}{\eta_{AC}} \left( P_{r,AC}^{\frac{k_{air}-1}{k_{air}}} - 1 \right) \right) \quad (11)$$

$$\dot{W}_{AC} = \dot{m}_{air} (h_{out} - h_{in}) \quad (12)$$

In this context, $\dot{m}_{air}$ and $k_{air}$ denote the mass flow rate and the specific heat ratio of the air, respectively. On the other hand, $\eta_{AC}$ represents the isentropic efficiency of the AC, while $P_{r,AC}$ stands for the pressure ratio. The following equations determine the gas turbine's output temperature and power generation [31]:

$$T_{GT,\,out} = T_{GT,\,in} \left( 1 - \eta_{GT} \left( 1 - P_{r,GT}^{\frac{1-k_{air}}{k_{air}}} \right) \right) \quad (13)$$

$$\dot{W}_{GT} = \dot{m}_{GT,in} * (h_{GT,\,in} - h_{GT,\,out}) \quad (14)$$

$$\dot{W}_{GT,net} = \eta_{GEN} * \left( \dot{W}_{GT} - \dot{W}_{AC} \right) \quad (15)$$

The equation uses $\eta_{GT}$, $P_{r,GT}$, $\eta_{GEN}$, $\dot{m}_{GT,in}$ to represent the turbine isentropic efficiency, turbine pressure ratio, generator efficiency, and combustion gas flow rate.

Determining the heat loss from the tank to the ambient is a key part of the thermodynamic model used to calculate the RB storage tank. First, we use the below equation to get the total heat loss from the store to the ambient air, and then we compute the total heat loss coefficient (U):

$$\dot{Q}_{loss} = U \times A \times (T_m - T_0) \quad (16)$$

where $T_0$ and $T_m$ are the ambient and mean temperatures (in °C), and A is the total surface area of the RB storage tank.

The RBES operates in three modes: charging, discharging, and storage. The following formulas determine the total energy stored when charging [15]:

$$Q_{\,charging} = (m_5 h_5 - m_6 h_6) \times 3600 \times t_{charging} \quad (17)$$

$$Q_{charging} = m_{rock}\, c_{rock} (T_5 - T_0) \quad (18)$$

where $c_{rock}$ is the rock's specific heat, $t_{charging}$ is the charging time, and $m_{rock}$ is the rock's mass. To calculate the overall heat loss throughout the storage time, one uses the following equation:

$$Q_{charging} = Q_{discharging} + Q_{loss} \quad (19)$$

The heat delivered to the Rankine cycle during the discharge time is determined using the following formula [15]:

$$Q_{discharging} = (m_7 h_7 - m_9 h_9) \times 3600 \times t_{discharging} \quad (20)$$

$$Q_{discharging} = m_{rock}\, c_{rock}\, (T_5 - T_0) \quad (21)$$

where $t_{discharging}$ is the discharging time (in s). Table 3 presents the energy and exergy equations for the CCPP's components. Table 4 shows the exergy of the fuel and the product for each component.

**Table 3.** The equations related to energy and exergy balance in a CCPP.

| Component | Energy Balance Equation | Exergy Balance Equation |
|---|---|---|
| AC | $\dot{m}_1\, h_1 + \dot{W}_{AC} = \dot{m}_2\, h_2$ | $\dot{E}_{D,AC} = \left(\dot{E}_1 - \dot{E}_2\right) + \dot{W}_{AC}$ |
| SR | $\dot{m}_2\, h_2 + \dot{Q}_{SR} = \dot{m}_3\, h_3$ | $\dot{E}_{D,SR} = \left(\dot{E}_2 - \dot{E}_3\right) + \dot{E}_{Q,Solar}$ |
| CC | $\dot{m}_3\, h_3 + \eta_{CC} \dot{m}_f LHV_f = \dot{m}_4 h_4$ | $\dot{E}_{D,CC} = \dot{E}_3 + \dot{E}_{Q,_{Fuel}} - \dot{E}_4$ |
| GT | $\dot{m}_4 h_4 = \dot{m}_5 h_5 + \dot{W}_{GT}$ | $\dot{E}_{D,GT} = \left(\dot{E}_4 - \dot{E}_5\right) - \dot{W}_{GT}$ |
| RBES Charging | $(m_5 h_5 - m_6 h_6) \times 3600 \times t_{charging} = m_{rock}\, c_{rock} (T_5 - T_0)$ | $\left(\dot{E}_5 - \dot{E}_6\right) \times 3600 \times t_{charging} = m_{rock}\, c_{rock}\, ((T_5 - T_0)\ -T_0 \times \ln\left(\frac{T_5}{T_0}\right)) + \dot{E}_{D,charging} \times 3600 \times t_{charging}$ |
| RBES Discharging | $(m_7 h_7 - m_9 h_9) \times 3600 \times t_{discharging} = m_{rock}\, c_{rock} (T_5 - T_0)$ | $\left(\dot{E}_7 - \dot{E}_9\right) \times 3600 \times t_{discharging} + \dot{E}_{D,discharging} \times 3600 \times t_{discharging} = m_{rock}\, c_{rock}\, ((T_5 - T_0) - T_0 \times \ln(T_5/T_0))$ |
| Blower | $\dot{m}_8\, h_8 + \dot{W}_{blower} = \dot{m}_9\, h_9$ | $\dot{E}_{D,blower} = \left(\dot{E}_8 - \dot{E}_9\right) + \dot{W}_{blower}$ |
| Boiler | $\dot{m}_7 (h_7 - h_8) = \dot{m}_{10} (h_{10} - h_{13})$ | $\dot{E}_{D,Boiler} = \dot{E}_7 - \dot{E}_8 + \dot{E}_{13} - \dot{E}_{10}$ |
| ST | $\dot{m}_{10} h_{10} = \dot{m}_{11} h_{11} + \dot{W}_{ST}$ | $\dot{E}_{D,ST} = \left(\dot{E}_{10} - \dot{E}_{11}\right) - \dot{W}_{ST}$ |
| Condenser | $\dot{m}_{11} (h_{11} - h_{12}) = \dot{m}_{14} (h_{15} - h_{14})$ | $\dot{E}_{D,cond} = \dot{E}_{11} - \dot{E}_{12} + \dot{E}_{14} - \dot{E}_{15}$ |
| Pump | $\dot{m}_{12}\, h_{12} + \dot{W}_{pump} = \dot{m}_{13}\, h_{13}$ | $\dot{E}_{D,pump} = \left(\dot{E}_{12} - \dot{E}_{13}\right) + \dot{W}_{pump}$ |

**Table 4.** The equations related to product and fuel exergy.

| Component | Fuel Exergy Equation | Product Exergy Equation |
|---|---|---|
| AC | $\dot{W}_{AC}$ | $\dot{E}_2 - \dot{E}_1$ |
| SR | $\dot{E}_{Q,Solar}$ | $\dot{E}_3 - \dot{E}_2$ |
| CC | $\dot{E}_{Q,_{Fuel,}}$ | $\dot{E}_4 - \dot{E}_3$ |
| GT | $\dot{E}_4 - \dot{E}_5$ | $\dot{W}_{GT}$ |
| RBES charging | $\dot{E}_5 - \dot{E}_6$ | $m_{rock}\, c_{rock}\, ((T_5 - T_0) - T_0 \times \ln\left(\frac{T_5}{T_0}\right)) / (3600 \times t_{charging})$ |
| RBES discharging | $m_{rock}\, c_{rock}\, ((T_5 - T_0) - T_0 \times \ln\left(\frac{T_5}{T_0}\right)) / (3600 \times t_{discharging})$ | $\dot{E}_7 - \dot{E}_9$ |
| Blower | $\dot{W}_{blower}$ | $\dot{E}_9 - \dot{E}_8$ |
| Boiler | $\dot{E}_7 - \dot{E}_8$ | $\dot{E}_{10} - \dot{E}_{13}$ |
| ST | $\dot{E}_{10} - \dot{E}_{11}$ | $\dot{W}_{ST}$ |
| Condenser | $\dot{E}_{11} - \dot{E}_{12}$ | $\dot{E}_{15} - \dot{E}_{14}$ |
| Pump | $\dot{W}_{pump}$ | $\dot{E}_{13} - \dot{E}_{12}$ |

The efficiency of the CCPP is calculated by analyzing the first and second laws [32]:

$$\eta_I = \frac{\dot{W}_{net}}{\dot{Q}_{in}} \quad (22)$$

$$\eta_{II} = \frac{\dot{W}_{net}}{\dot{E}_{in}} \quad (23)$$

The net power of the CCPP is determined by the following equation:

$$\dot{W}_{net} = \dot{W}_{GT} - \dot{W}_{Comp} + \dot{W}_{ST} - \dot{W}_{Pump} - \dot{W}_{Blower} \quad (24)$$

The CCPP's heat and exergy input are calculated as follows:

$$\dot{Q}_{in} = \dot{Q}_{Fuel} + \dot{Q}_{Solar} \quad (25)$$

$$\dot{E}_{in} = \dot{E}_{Q,Fuel} + \dot{E}_{Solar} \quad (26)$$

## 4. Exergy Economic Analysis

The following equation describes the overall system-wide exergy-cost balance for all the system components [33]:

$$\sum \dot{C}_{in,k} + \dot{C}_{Q,k} + \dot{Z}_k = \sum \dot{C}_{out,k} + \dot{C}_{w,k} \quad (27)$$

The heat and power exergy cost flows are denoted as $\dot{C}_{Qk}$ and $\dot{C}_{w,k}$ correspondingly, whereas $\dot{Z}_k$ represents the capital cost. The calculation of $\dot{Z}_k$ is based on the formula shown below [34,35]:

$$\dot{Z}_k = Z_k * CRF * \frac{\phi}{t} \quad (28)$$

The referenced equations used to determine the investment cost of the components, denoted by $Z_k$, are derived from references. $\phi$ denotes the maintenance factor, and t stands for the yearly running time of the CCPP [13,36,37]. This study assumes a total annual working time of 8640 h. CRF represents the return on capital factor, and it is calculated using the following equation [38]:

$$CRF = \frac{i(1+i)^N}{(1-i)^N - 1} \quad (29)$$

The interest rate, denoted as i, is fixed at 12%, while N denotes the CCPP's overall lifespan, which is 20 years [39]. The exergy cost flow for each location in the CCPP is determined using the following formula:

$$\dot{C} = c\dot{E} \quad (30)$$

where c represents the specific exergy cost, and $\dot{E}$ indicates the exergy current. The CCPP's performance is assessed using the exergy-economic factor, designated as $f_k$, which is determined using the following equation [40]:

$$f_k = \frac{\dot{Z}_k}{\dot{Z}_k + \dot{C}_{D,k}} \quad (31)$$

The exergy destruction cost, denoted as $\dot{C}_{D,k}$, is determined using the following equation [40]:

$$\dot{C}_{D,k} = c_f \dot{E}_{D,k} \quad (32)$$

where $\dot{E}_{D,k}$ is the exergy destruction. Table 5 contains all the auxiliary equations that are linked to the cost equilibrium equations. The total cost of the CCPP system ($\dot{C}_{system}$) can be calculated utilizing the following equation [41,42]:

$$\dot{C}_{system} = \sum \dot{Z}_k + \sum \dot{C}_{D,k} \tag{33}$$

**Table 5.** Equations for cost balancing system elements.

| Component | Cost Flow Equations | Auxiliary Equations |
|---|---|---|
| AC | $\dot{C}_1 + \dot{C}_{AC} + \dot{Z}_{AC} = \dot{C}_2$ | $c_1 = 0$ |
| SR | $\dot{C}_2 + \dot{Z}_{hel} = \dot{C}_3$ | $c_2 = c_3$ |
| CC | $\dot{C}_3 + \dot{C}_{fuel} + \dot{Z}_{CC} = \dot{C}_4$ | $c_3 = c_4$<br>$c_f = 12$ |
| GT | $\dot{C}_4 + \dot{Z}_{GT} = \dot{C}_5 + \dot{C}_{GT}$ | $c_4 = c_5$<br>$c_{AC} = c_{GT}$ |
| RBES | $\dot{C}_5 + \dot{C}_9 + \dot{Z}_{RBES} = \dot{C}_6 + \dot{C}_7$ | $c_5 = c_6$ |
| Blower | $\dot{C}_9 + \dot{C}_{Blower} + \dot{Z}_{Blower} = \dot{C}_{10}$ | $c_{blower} = c_{GT}$ |
| Boiler | $\dot{C}_7 + \dot{C}_{13} + \dot{Z}_{Boiler} = \dot{C}_8 + \dot{C}_{10}$ | $c_7 = c_8$ |
| ST | $\dot{C}_{10} + \dot{Z}_{ST} = \dot{C}_{11} + \dot{C}_{ST}$ | $c_{10} = c_{11}$ |
| Condenser | $\dot{C}_{11} + \dot{C}_{14} + \dot{Z}_{Condenser} = \dot{C}_{12} + \dot{C}_{15}$ | $c_{12} = c_{13}$<br>$c_{14} = 0$ |
| Pump | $\dot{C}_{12} + \dot{C}_{Pump} + \dot{Z}_{pump} = \dot{C}_{13}$ | $c_{Pump} = c_{ST}$ |

The system's unit cost of electricity produced ($\dot{C}_{electricity}$) is another important aspect in the cost analysis. The equation provided calculates the overall cost of the power generated [43,44]:

$$\dot{C}_{electricity} = \frac{\dot{C}_{system}}{\dot{W}_{net}}$$

## 5. Environmental Assessment

The $CO_2$ emission rate ($\epsilon_{CO_2}$) measures the amount of $CO_2$ that is emitted into the atmosphere as a result of human activities [45,46]. The value of $\epsilon_{CO_2}$ for electricity production is calculated by dividing the total amount of $CO_2$ emissions produced during a certain period of time by the total amount of energy generated during the same period. The rate is calculated using the following equation [47,48]:

$$\epsilon_{CO_2} = \frac{\dot{m}_{CO_2}}{\dot{W}_{net}} \tag{34}$$

The estimation of the mass flow rate of $CO_2$ is determined using the following equation [49]:

$$\dot{m}_{CO_2} = y_{CO_2} \dot{m}_{g,5} \left( \frac{\overline{M}_{CO_2}}{\overline{M}_g} \right) \tag{35}$$

where $\dot{m}_{CO_2}$ represents the molecular weight of $CO_2$, whereas $\overline{M}_{CO_2}$ represents the mole fraction of $CO_2$. Furthermore, $\dot{m}_g$ represents the molecular weight of the exhaust gases, whereas $\overline{M}_g$ denotes the mole fraction of the exhaust gases after the combustion chamber.

## 6. Results and Discussion

The results of analyzing the energy, exergy, and cost balance equations for each of the developed cycle's constituent components are shown in this section. Table 6 provides details of the calculated and assumed properties for all the state points. The calculations related to exergy destruction and capital investment costs are performed.

**Table 6.** Thermodynamic characteristics of the solar-powered combined cycle in each of its ideal states.

| State | $\dot{m}$ (kg/s) | T (K) | P (kPa) | h (kJ/kg) | S (KJ/kg. K) | $\dot{E}$ (MW) | $\dot{C}$ ($/h) | c ($/GJ) |
|---|---|---|---|---|---|---|---|---|
| 1 | 52 | 306.7 | 101.3 | 307.1 | 5.724 | 0.0633 | 0 | 0 |
| 2 | 52 | 711.7 | 1469 | 726.2 | 5.823 | 20.33 | 117.4 | 1.604 |
| 3 | 52 | 1172 | 1469 | 1245 | 6.383 | 38.64 | 223.1 | 1.604 |
| 4 | 52 | 1273 | 1469 | 1364 | 6.48 | 43.31 | 427.5 | 2.742 |
| 5 | 52 | 752.1 | 108.8 | 770 | 6.63 | 10.1 | 99.68 | 2.742 |
| 6 | 52 | 382.3 | 101.3 | 383.4 | 5.946 | 0.5848 | 5.773 | 2.742 |
| 7 | 37.51 | 742.1 | 107 | 759.1 | 6.62 | 6.986 | 113.2 | 4.503 |
| 8 | 37.51 | 343.2 | 107 | 343.9 | 5.822 | 0.3334 | 5.404 | 4.503 |
| 9 | 37.51 | 375.3 | 140 | 376.3 | 5.835 | 1.403 | 19.04 | 3.769 |
| 10 | 5.092 | 722.1 | 5000 | 3315 | 6.818 | 6.557 | 155.6 | 6.592 |
| 11 | 5.092 | 333 | 19.81 | 2459 | 7.46 | 1.222 | 29.01 | 6.592 |
| 12 | 5.092 | 333 | 19.81 | 250.6 | 0.8294 | 0.0407 | 0.966 | 6.592 |
| 13 | 5.092 | 333.2 | 5000 | 256.2 | 0.8311 | 0.0667 | 2.61 | 10.86 |
| 14 | 269 | 306.7 | 101.3 | 140.4 | 0.4847 | 0.139 | 0 | 0 |
| 15 | 269 | 316.7 | 101.3 | 182.2 | 0.6189 | 0.6315 | 28.19 | 12.4 |

The monthly fluctuations in the CCPP's power output and energy cost rate will be provided. The thermodynamic model employed in this research for the developed cycle has undergone cross-verification using the findings from a study conducted by Oztürk et al. [15], as demonstrated in Figure 3. The outcomes of this study closely align with the existing literature.

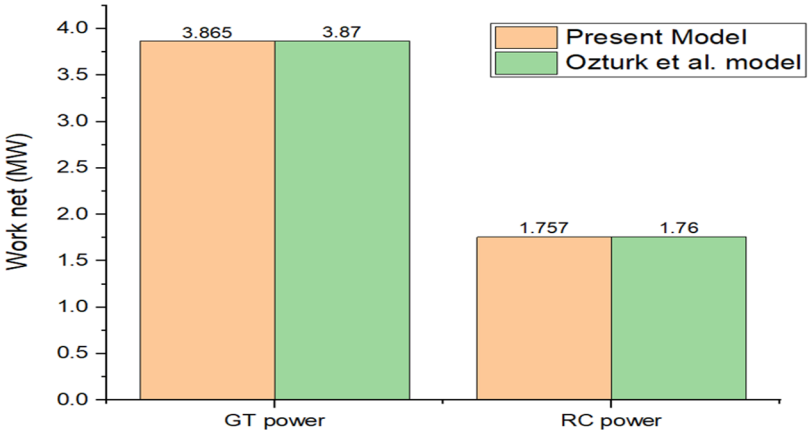


**Figure 3.** Comparative analysis between the present thermodynamic model vs. Oztürk et al.'s published work [15].

Exergy destruction inside the CCPP components under ideal operating circumstances is explained in Table 7 and Figure 4. High-temperature variances correlate with more significant exergy destruction. Solar receivers experience the most significant temperature difference, and they exhibit the highest destruction rate, amounting to 7.346 MW. GT and CC also contribute significantly to the overall destruction, accounting for 13.98% and 10.41%, respectively. Figure 3 highlights the pronounced exergy destruction in the GT. This phenomenon is attributed to the impact of hot air on its turbine blades. Rock bed

energy storage (RBES) contributes 10.13% due to charging and discharging processes. AC, condensers, and ST played roles in the overall destruction. The pump exhibits minimal contributions. The boiler achieves an impressive exergy efficiency of 97.6%. These findings shed light on the intricate dynamics of exergy destruction and utilization within the system.

**Table 7.** An examination of the exergy analysis of the CCPP.

| Component | $\dot{E}_{input}$ (MW) | $\dot{E}_{output}$ (MW) | $\dot{E}_{destruction}$ (MW) | $\dot{E}_{destruction}$ (%) | Exergy Efficiency (%) |
|---|---|---|---|---|---|
| AC | 21.97 | 20.26 | 1.528 | 9.237 | 92.99 |
| Blower | 1.215 | 1.07 | 0.1455 | 0.88 | 88.03 |
| Boiler | 6.653 | 6.49 | 0.1625 | 0.98 | 97.56 |
| CC | 6.392 | 4.668 | 1.724 | 10.411 | 73.04 |
| Condenser | 1.182 | 0.4925 | 0.6893 | 4.165 | 41.67 |
| GT | 33.21 | 30.9 | 2.314 | 13.98 | 93.03 |
| Pump | 0.02863 | 0.0261 | 0.00256 | 0.015 | 91.06 |
| RBES | 15.15 | 13.47 | 1.677 | 10.132 | 88.9 |
| RBES charging | 9.514 | 7.89 | 1.624 | 9.812 | 82.93 |
| RBES discharging | 5.635 | 5.583 | 0.053 | 0.32 | 99.07 |
| SR | 25.66 | 18.32 | 7.346 | 44.4 | 43.94 |
| ST | 5.334 | 4.359 | 0.9572 | 5.8 | 81.72 |
| Total | | | 16.55 | | |

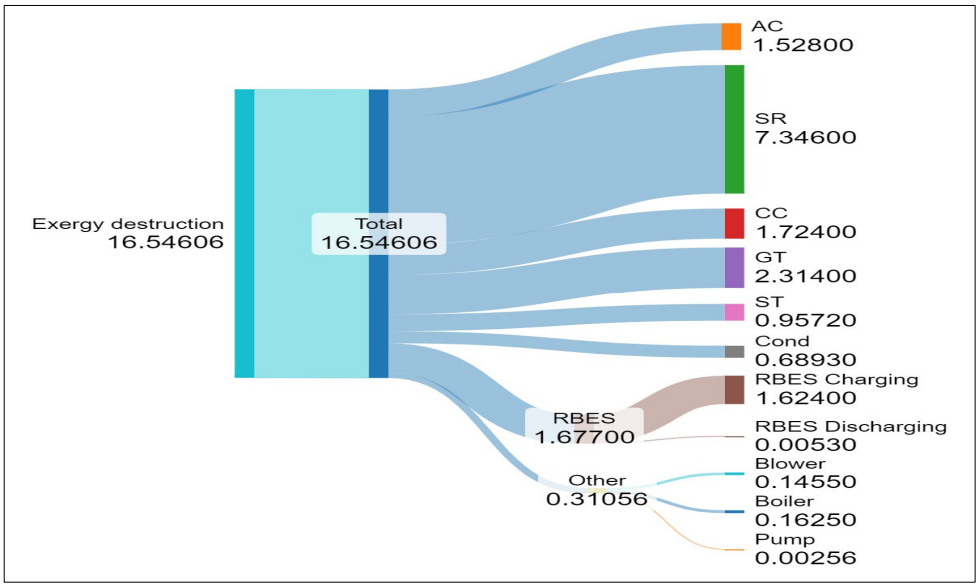


**Figure 4.** Exergy degradation rates of system components.

The designed cycle's exergoeconomic characteristics are shown in Table 8. Among all the components, the solar receiver incurs the greatest capital cost rate, amounting to 105.8 USD/h. The steam turbine and combustion chamber follow the solar receiver, with capital costs of 56.09 USD/h and 55.23 USD/h, respectively. The boiler, air compressor, and gas turbine also have relatively high capital costs. The CCPP's exergy destruction cost rate is crucial for exergoeconomic analysis. The CC has the highest exergy destruction cost rate at 55.07 USD/h, followed by the GT. Interestingly, the capital cost rate of the entire system surpasses the total cost rate of exergy destruction. The components with the highest values are considered the most significant. The solar receiver (SR) stands out with the maximum

value of $\dot{Z}_k + \dot{C}_D$, while the steam turbine (ST) comes in second. The CCPP demonstrates an exceptionally high exergoeconomic factor of 63.07%. These insights provide valuable information for assessing the economic and energetic aspects of the system.

**Table 8.** Designed cycle's exergoeconomic characteristics.

| Component | $c_f$ ($/GJ) | $c_p$ ($/GJ) | $\dot{C}_D$ ($/h) | $\dot{Z}_K$ ($/h) | $\dot{Z}_K+\dot{C}_D$ ($/h) | f (%) |
|---|---|---|---|---|---|---|
| AC | 1.022 | 1.609 | 5.625 | 37.185 | 42.81 | 86.86 |
| Blower | 3.061 | 3.54 | 1.603 | 0.244 | 1.847 | 13.18 |
| Boiler | 4.503 | 6.549 | 2.634 | 45.336 | 47.97 | 94.94 |
| CC | 8.875 | 12.16 | 55.07 | 0.16 | 55.23 | 0.302 |
| Condenser | 6.592 | 15.9 | 16.36 | 0.14 | 16.5 | 0.8516 |
| GT | 2.724 | 3.061 | 22.84 | 12.62 | 35.46 | 35.59 |
| Pump | 10.17 | 17.52 | 0.0937 | 0.5962 | 0.6899 | 86.42 |
| RBES | 1.722 | 1.942 | 10.39 | 0.3 | 10.69 | 2.816 |
| SR | - | 1.604 | - | 105.8 | 105.8 | 100 |
| ST | 6.592 | 10.17 | 23.15 | 32.94 | 56.09 | 58.74 |
| Total system | | | 137.76 | 235.32 | 373.08 | 63.07 |

Figure 5a,b illustrate the influence of ambient temperature ($T_1$) on various performance metrics. As ($T_1$) increases, a decrease is observed in the network output $\left(\dot{W}_{net}\right)$, the system power cost rate $\left(\dot{C}_{electricity}\right)$, the overall system efficiency ($\eta_I$), and the second-law efficiency ($\eta_{II}$). This trend is mainly attributed to the rising enthalpy ($h_2$) and the power consumption of the air compressor with increasing $T_1$. A portion of $\dot{W}_{net}$ powers the compressor, and the rise in $\dot{W}_{AC}$ negatively impacts both the $\dot{W}_{net}$ and overall efficiencies. Figure 5a quantifies this effect, showing a decrease in $\dot{W}_{net}$ from 13,382 kW to 11,641 kW when $T_1$ increases from 290 K to 315 K. When the ambient temperature decreases, both the work consumed by the compressor and the exit temperature of the compressor decrease. Consequently, the air temperature entering the combustion chamber also decreases. This decrease in inlet temperature increases the cost of exergy destruction in the combustion chamber and the entire cycle, which raises the specific energy cost. Figure 5a highlights this trend, with $\dot{C}_{electricity}$ decreasing from 31.21 USD/MWh to 30.26 USD/MWh as $T_1$ increases from 290 K to 315 K. Furthermore, Figure 5b demonstrates the corresponding decline in efficiencies. $\eta_I$, representing the system's overall efficiency, decreases from 38.01% to 36.2%, and $\eta_{II}$, reflecting the second-law efficiency, decreases from 41.9% to 39.31%.

Figure 6a,b illustrate how the pressure ratio (PR) impacts various aspects of the combined cycle power plant. As the PR increases, the system's power output decreases. Specifically, when the PR rises from 8 to 20, the $\dot{W}_{net}$ decreases significantly from 14.04 MW to 10.445 MW (a reduction of around 3.594 MW), as seen in Figure 6a. This reduction is primarily due to the increased work of the air compressor. Elevating the PR to 15 results in a reduction in the system's electricity cost rate. The cost rate decreases from 34.38 USD/MWh to 30.49 USD/MWh. This reduction is attributed to the decrease in the $\dot{W}_{net}$ and the fuel input rate. Interestingly, when the PR surpasses 15, the cycle's energy cost rate begins to climb. This upward trend is primarily due to the significant drop in the $\dot{W}_{net}$. Figure 6b demonstrates that as the pressure ratio (PR) increases, the system efficiencies improve until they peak. Beyond this point, the efficiency declines. At higher PR values, a decrease in the $\dot{W}_{net}$ negatively affects the overall system efficiencies. At 13 bars, the maximum thermal

efficiency reached 36.9%, while the maximum exergy efficiency of 40.66% was achieved at 11.4 bar.

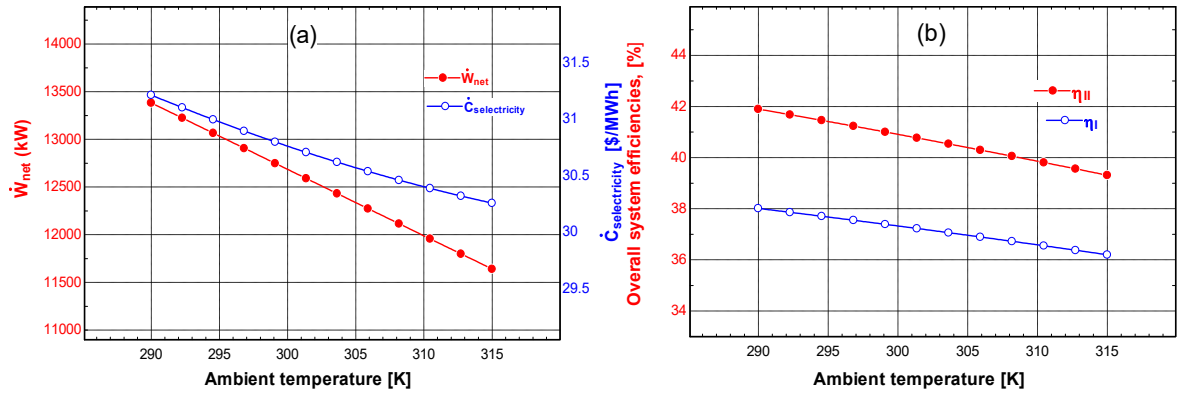


**Figure 5.** The impact of the ambient temperature ($T_1$) change on the system's work output, power cost rate, and overall efficiency.

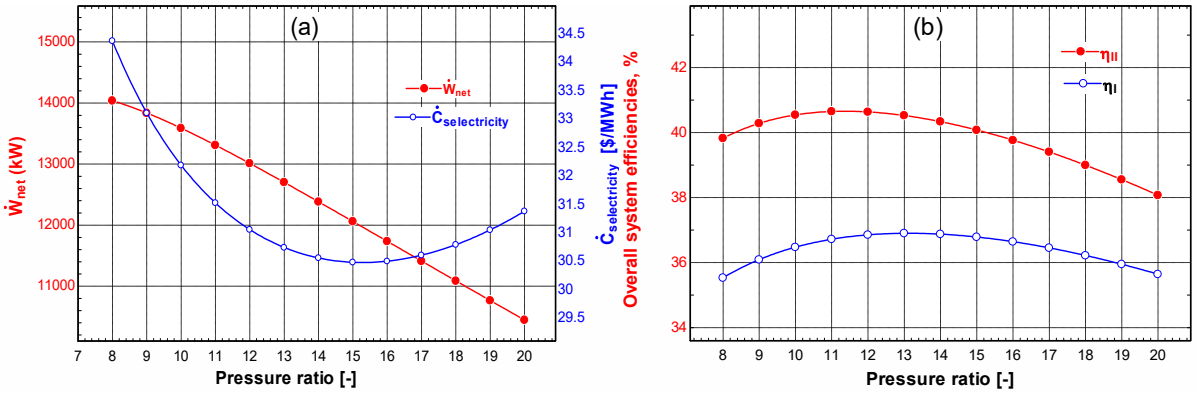


**Figure 6.** The impact of pressure ratio (PR) changes on the system's work output, power cost rate, and overall efficiency.

The effect of the GTIT ($T_4$) on the power output, the cycle's energy cost rate, and the overall efficiencies of the system according to the first and second laws are depicted in Figure 7a,b. Increasing $T_4$ improves the cycle's power output and overall efficiencies. The CCPP achieved its greatest energy and exergy overall efficiencies of 38.39% and 42.294%, respectively, at 1050 K, as presented in Figure 7b. As $T_4$ rises, the energy and exergy inputs to the gas turbine increase. Notably, an elevated $T_4$ significantly enhances energy storage in the rock bed energy storage (RBES), improving the overall efficiency and power output. When $T_4$ rises from 800 K to 1050 K, the power output experiences a substantial increase. Specifically, the power output increased from 5590 kW to 13,922 kW (an increase of approximately 8332 kW). The study reveals that $T_4$ significantly affects the CCPP's electricity cost rate. Figure 7a demonstrates that as $T_4$ increases, the CCPP's power cost rate decreases. The findings suggest that the system's electricity cost was reduced from 32.15 to 30.47 USD/MWh. These insights provide valuable information for optimizing the system's performance and cost-effectiveness.

Figure 8 depicts how the sun and backup fuel contribute to the CCPP's yearly heat supply. The data reveal that the summer months benefit from the sun's increased intensity, with solar energy providing a whopping 81.42% of the heat in June. Conversely, the winter presents a different version. Due to lower solar radiation, the system relies heavily on fuel for heat, with solar only accounting for 44.41% of the needs in December. In essence, the sun plays the leading role in heat generation during the summer, while fuel becomes more crucial in the winter.

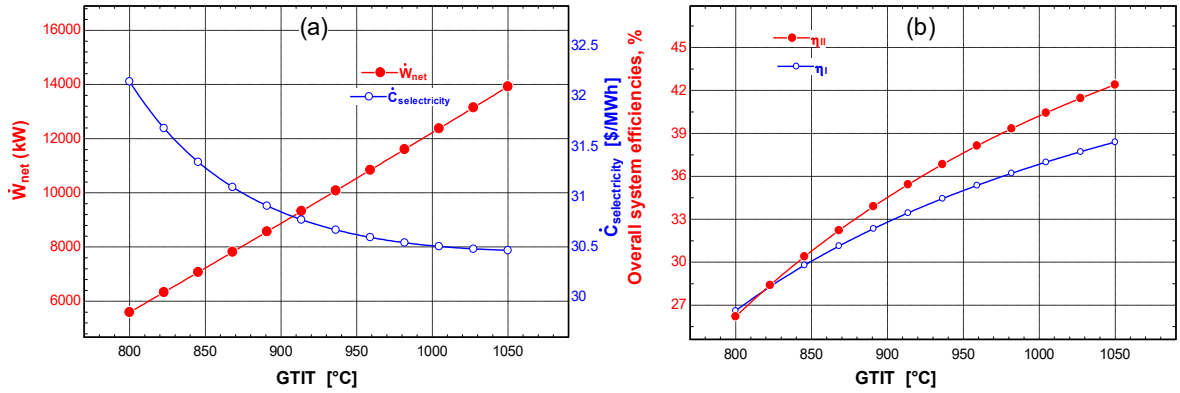


**Figure 7.** The impact of the gas turbine inlet temperature ($T_4$) changes on the system's work output, energy cost rate, and overall efficiencies.

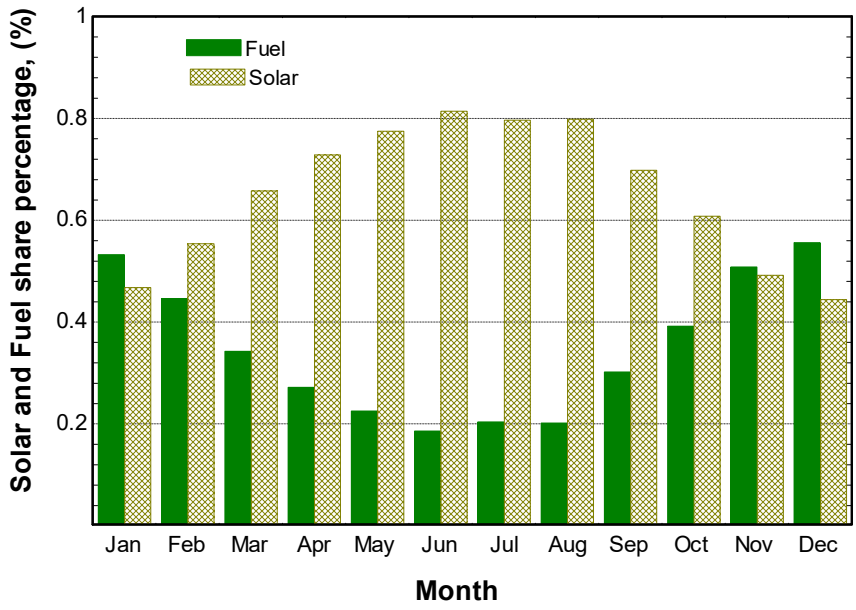


**Figure 8.** Changes in solar and fuel shares across each month.

Figure 9 illustrates the CCPP's power output variation across the year. Interestingly, January sees the highest power generation, reaching 13,276 kW. This can be attributed to two factors. First, fuel delivers higher quality energy compared to solar energy. Second, colder environments favor the gas turbine cycle's efficiency. Due to these reasons, the system produces more power in January than in August, which sees a lower output of 12,206 kW.

Figure 10 shows how this CCPP's electricity cost changes throughout the year. Interestingly, it is cheaper in the summer compared to the winter. This is because summer sunshine provides most of the power, and sunshine is free! The data present that the energy cost rate is as low as 30.36 USD/MWh in June but increases to 46.76 USD/MWh in December.

Figure 11 illustrates the annual variation in $CO_2$ emissions for this system. Overall, the system maintains a very low carbon footprint due to its reliance on clean energy sources and minimal fuel usage. Interestingly, the carbon footprint is lower during the winter months compared to the summer. This is attributed to the system generating more power in January than in August. Specifically, the data reveal $CO_2$ emission rates as low as 0.1 kg/kWh in January, rising to 0.11 kg/kWh in August.

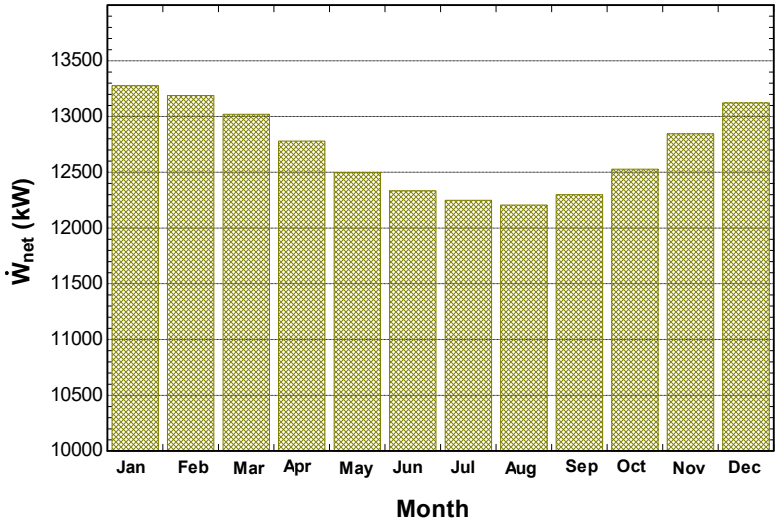


**Figure 9.** Changes in the CCPP's work net across each month.

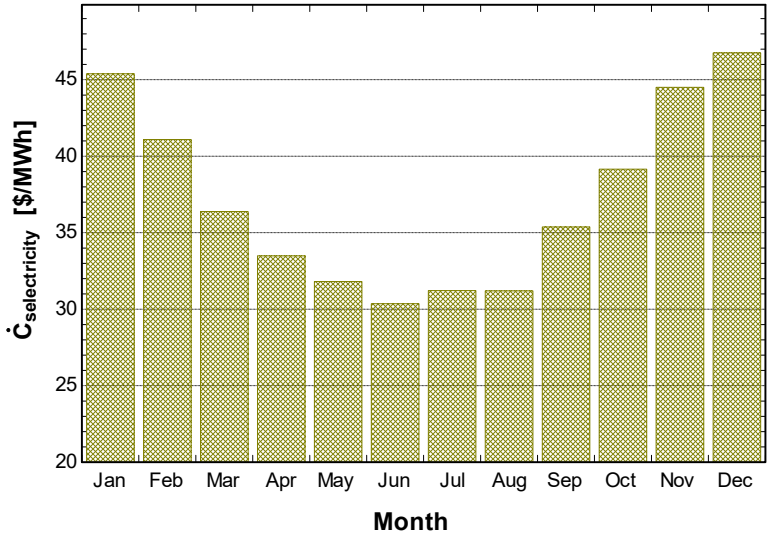


**Figure 10.** Changes in the CCPP's electricity cost rate across each month.

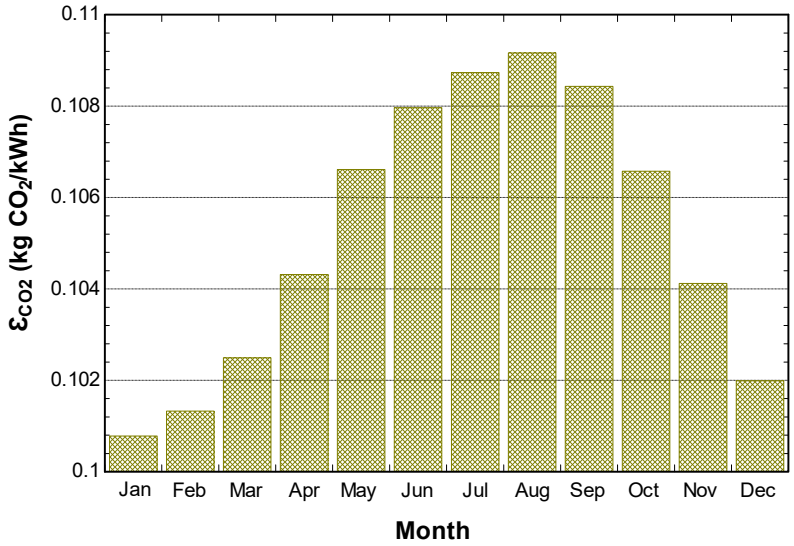


**Figure 11.** Changes in $CO_2$ emissions across each month.

## 7. Conclusions

This study explored an innovative power generation system integrating a solar combined cycle system with fossil fuel and rock bed thermal energy storage in Neom City, Saudi Arabia. The investigation centered on thermodynamics, specifically energy, exergy, exergoeconomic, and environmental analysis. This distinctive configuration merges RBES with two power cycles: a solar Brayton cycle and a steam Rankine cycle. Over ten hours, the heated exhaust gas from the solar Brayton cycle powers the RBES, which uses this stored energy to run the RC for fourteen hours. The research scrutinized how vital parameters such as ambient temperature, pressure ratios within the cycles, and the GTIT influence electricity production's comprehensive performance and cost. The study led to several noteworthy conclusions, as follows:

- In the CCPP powered by SE, the system's power output reaches a peak of 13,276 kW in January and decreases to its lowest output of 12,206 kW in August.
- The CCPP's power cost is greater during the winter than in the summer. Specifically, it was 30.35 USD/MWh in June, while it escalated to 46.76 USD/MWh in December.
- The exergoeconomic factor ($f_k$) performs a crucial role in the analysis of exergy economics. The designed CCPP system boasts an impressive exergoeconomic factor, peaking at 63.07%. This significant figure will likely motivate the Saudi Arabian government to construct this CCPP.
- The designed system has a lower carbon impact due to clean energy and efficient fuel use. $CO_2$ emission rates vary from 0.1 kg $CO_2$/kWh in January to 0.11 kg $CO_2$/kWh in August.
- The system's performance and cost are notably influenced by the ambient temperature, a factor that warrants careful consideration during the system's design phase.
- An increase in the GTIT notably enhances the system's performance and efficiencies while concurrently reducing the system's electricity cost rate.

**Author Contributions:** Conceptualization, A.A. and A.S.A.S.; Methodology, A.A.; Formal analysis, A.A.; Investigation, A.A. and A.S.A.S.; Resources, A.A. and A.S.A.S.; Data curation, A.A.; Writing—original draft, A.A.; Writing—review and editing, A.A. and A.S.A.S.; Funding acquisition, A.S.A.S. All authors have read and agreed to the published version of the manuscript.

**Funding:** This work was supported by the Deanship of Scientific Research, Vice Presidency for Graduate Studies and Scientific Research, King Faisal University, Saudi Arabia (Grant No. KFU241351).

**Data Availability Statement:** The data are contained within the article.

**Acknowledgments:** All the authors are grateful to King Faisal University and Karabuk University for providing their software (https://fchartsoftware.com/ees/) and hardware infrastructure to realize the current study.

**Conflicts of Interest:** The authors declare no conflicts of interest.

## Nomenclature

| | |
|---|---|
| $\dot{E}$ | exergy rate (kJ/s) |
| $h_c$ | convective heat transfer coefficient of air (W/m$^2$K) |
| $\dot{W}$ | power (kW) |
| $\dot{Z}$ | capital cost (USD/h) |
| $A_{ap}$ | area of the solar field (m$^2$) |
| $\dot{C}$ | cost rate (USD/h) |
| $\dot{Q}$ | heat transfer rate (kW) |
| $\dot{S}$ | entropy rate (W/K) |
| $T_{sun}$ | sun temperature |
| $\dot{m}$ | mass flow rate (kg/s) |
| c | specific heat (kJ kg$^{-1}$ K$^{-1}$) |
| DNI | direct normal irradiance of the sun |

| | |
|---|---|
| e | specific exergy (kJ/kg) |
| h | specific enthalpy (kJ. $kg^{-1}$) |
| k | specific heat ratio |
| LHV | fuel's lower heating value (kJ/kg) |
| m | mass (kg) |
| N | number of operating hours |
| P | pressure (kPa) |
| Q | heat transfer (kJ) |
| s | specific entropy (kJ $kg^{-1}$ $K^{-1}$) |
| t | time (s) |
| T | temperature |
| U | overall heat transfer coefficient ($W/m^2K$) |
| V | wind velocity (m/s) |
| Greek Symbols | |
| i | interest rate |
| η | energy efficiency |
| Ψ | exergy efficiency |
| f | exergy-economic factor |
| ε | emissivity |
| σ | Stefan–Boltzmann constant |
| φ | maintenance factor |
| Subscripts | |
| c | convection |
| D | destruction |
| f | fuel |
| h | heliostat |
| in | inlet |
| k | component |
| O | reference state |
| out | exit |
| p | product |
| q | related to heat |
| r | radiation |
| tot | total |
| w | related to work |
| **Abbreviations** | |
| AC | air compressor |
| CC | combustion chamber |
| CRF | capital recovery factor |
| CSP | concentration solar power |
| GT | gas turbine |
| GTC | gas turbine cycle |
| GTIT | gas turbine inlet temperature |
| HE | heat exchanger |
| Pr | pressure ration |
| RBES | rock bed energy storage |
| SR | solar receiver |
| ST | steam turbine |
| TES | thermal energy storage |

## References

1. Ma, Z.; Glatzmaier, G.C.; Kutscher, C.F. Thermal energy storage and its potential applications in solar thermal power plants and electricity storage. In Proceedings of the ASME 2011 5th International Conference on Energy Sustainability, ES, Washington, DC, USA, 7–10 August 2011; Volume 2011, pp. 447–456. [CrossRef]
2. Talal, W.; Akroot, A. An Exergoeconomic Evaluation of an Innovative Polygeneration System Using a Solar-Driven Rankine Cycle Integrated with the Al-Qayyara Gas Turbine Power Plant and the Absorption Refrigeration Cycle. *Machines* **2024**, *12*, 133. [CrossRef]

3. Strielkowski, W.; Tarkhanova, E.; Tvaronavi, M.; Petrenko, Y. Renewable Energy in the Sustainable Development of Electrical. *Energies* **2021**, *14*, 8240. [CrossRef]
4. Delibaş, H.M.; Kayabaşı, E. Energy, Environment And Economy Assessment Of Waste Heat Recovery Technologies In Marine Industry. *Int. J. Mater. Eng. Technol.* **2019**, *4*, 39–45.
5. Kuravi, S.; Trahan, J.; Goswami, D.Y.; Rahman, M.M.; Stefanakos, E.K. Thermal energy storage technologies and systems for concentrating solar power plants. *Prog Energy Combust Sci* **2013**, *39*, 285–319. [CrossRef]
6. Soprani, S.; Marongiu, F.; Christensen, L.; Alm, O.; Dinesen, K.; Ulrich, T.; Engelbrecht, K. Design and testing of a horizontal rock bed for high temperature thermal energy storage. *Appl. Energy* **2019**, *251*, 113345. [CrossRef]
7. Desai, N.B.; Mondejar, M.E.; Haglind, F. Techno-economic analysis of two-tank and packed-bed rock thermal energy storages for foil-based concentrating solar collector driven cogeneration plants. *Renew. Energy* **2022**, *186*, 814–830. [CrossRef]
8. Marongiu, F.; Soprani, S.; Engelbrecht, K. Modeling of high temperature thermal energy storage in rock beds—Experimental comparison and parametric study. *Appl. Therm. Eng.* **2019**, *163*, 114355. [CrossRef]
9. Zanganeh, G.; Pedretti, A.; Zavattoni, S.; Barbato, M.; Steinfeld, A. Packed-bed thermal storage for concentrated solar power—Pilot-scale demonstration and industrial-scale design. *Sol. Energy* **2012**, *86*, 3084–3098. [CrossRef]
10. Nahhas, T.; Py, X.; Sadiki, N. Experimental investigation of basalt rocks as storage material for high- temperature concentrated solar power plants. *Renew. Sustain. Energy Rev.* **2019**, *110*, 226–235. [CrossRef]
11. Kocak, B.; Paksoy, H. Performance of laboratory scale packed-bed thermal energy storage using new demolition waste based sensible heat materials for industrial solar applications. *Sol. Energy* **2020**, *211*, 1335–1346. [CrossRef]
12. Sharma, A.; Pandey, P.K.; Didwania, M. Techno-economic optimization of packed-bed thermal energy storage system combined with CSP plant using DOE: Design of experiment technique and Taguchi method. *Int. J. Energy Environ. Eng.* **2022**, *14*, 287–308. [CrossRef]
13. Allen, K.; Heller, L.; von Backström, T. Cost Optimum Parameters for Rock Bed Thermal Storage at 550–600 C: A Parametric Study. *J. Sol. Energy Eng.* **2016**, *138*, 061004. [CrossRef]
14. Abdulla, A.; Reddy, K.S. Effect of operating parameters on thermal performance of molten salt packed-bed thermocline thermal energy storage system for concentrating solar power plants. *Int. J. Therm. Sci.* **2017**, *121*, 30–44. [CrossRef]
15. Ozturk, M.; Dincer, I. Thermodynamic analysis of a solar-based multi-generation system with hydrogen production. *Appl. Therm. Eng.* **2013**, *51*, 1235–1244. [CrossRef]
16. Cabrera, F.J.; Fernández-García, A.; Silva, R.M.P.; Pérez-García, M. Use of parabolic trough solar collectors for solar refrigeration and air-conditioning applications. *Renew. Sustain. Energy Rev.* **2013**, *20*, 103–118. [CrossRef]
17. Pelay, U.; Luo, L.; Fan, Y.; Stitou, D.; Rood, M. Thermal energy storage systems for concentrated solar power plants. *Renew. Sustain. Energy Rev.* **2017**, *79*, 82–100. [CrossRef]
18. Freeman, J.; Guarracino, I.; Kalogirou, S.A.; Markides, C.N. A small-scale solar organic Rankine cycle combined heat and power system with integrated thermal energy storage. *Appl. Therm. Eng.* **2017**, *127*, 1543–1554. [CrossRef]
19. Çam, N.Y.; Alptekin, E.; Bilir, L.; Ezan, M.A. Thermal behavior of a solar-assisted latent heat thermal energy storage unit on the heating season under variable weather conditions. *J. Energy Storage* **2022**, *52*, 104934. [CrossRef]
20. Khamlich, I.; Zeng, K.; Flamant, G.; Baeyens, J.; Zou, C.; Li, J.; Yang, X.; He, X.; Liu, Q.; Yang, H.; et al. Technical and economic assessment of thermal energy storage in concentrated solar power plants within a spot electricity market. *Renew. Sustain. Energy Rev.* **2021**, *139*, 110583. [CrossRef]
21. Al-Nimr, M.A.; Bukhari, M.; Mansour, M. A combined CPV/T and ORC solar power generation system integrated with geothermal cooling and electrolyser/fuel cell storage unit. *Energy* **2017**, *133*, 513–524. [CrossRef]
22. Shakouri, A.; Gorjian, S.; Ghobadian, B. Energy, exergy, and exergoeconomic (3E) evaluation of a hybrid multigeneration system based on a solar tower. *Appl. Therm. Eng.* **2024**, *252*, 123660. [CrossRef]
23. Kuterbekov, K.; Kabyshev, A.; Bekmyrza, K.; Kubenova, M. Energy, exergy and thermo-economics analyses of hybrid solar, steam turbine and biomass gasification system for hydrogen production by polymer membrane electrolyzer. *Int. J. Thermofluids* **2024**, *21*, 100556. [CrossRef]
24. Zhang, S.; Liu, M.; Zhao, Y.; Liu, J.; Yan, J. Energy and exergy analyses of a parabolic trough concentrated solar power plant using molten salt during the start-up process. *Energy* **2022**, *254*, 124480. [CrossRef]
25. Wang, G.; He, D.; Lin, J.; Jiang, T.; Chen, Z. Exergy estimate of a novel hybrid solar-gas power and organic Rankine cycle-based hydrogen-production system. *Case Stud. Therm. Eng.* **2022**, *33*, 124480. [CrossRef]
26. Moran, M.J.; Shapiro, H.N.; Boettner, D.D.; Bailey, M.B. *Fundamentals of Engineering Thermodynamics*; John Wiley & Sons: Hoboken, NJ, USA, 2020. [CrossRef]
27. Aghaziarati, Z.; Aghdam, A.H. Thermoeconomic analysis of a novel combined cooling, heating and power system based on solar organic Rankine cycle and cascade refrigeration cycle. *Renew. Energy* **2021**, *164*, 1267–1283. [CrossRef]
28. Tozlu, A.; Kayabasi, E.; Ozcan, H. Thermoeconomic analysis of a low-temperature waste-energy assisted power and hydrogen plant at off-NG grid region. *Sustain. Energy Technol. Assess.* **2022**, *52*, 102104. [CrossRef]
29. Yan, M.; Yao, Z.; Nutakki, T.U.K.; Agrawal, M.K.; Muhammad, T.; Albani, A.; Zhao, Z. Design and evaluation of a novel heliostat-based combined cooling, heating, and power (CCHP) system: 3E analysis and multi-criteria optimization by response surface methodology (RSM). *Energy* **2023**, *285*, 129389. [CrossRef]

30. Barakat, S.; Ramzy, A.; Hamed, A.M.; El Emam, S.H. Enhancement of gas turbine power output using earth to air heat exchanger (EAHE) cooling system. *Energy Convers Manag.* **2016**, *111*, 137–146. [CrossRef]
31. Abudu, K.; Igie, U.; Roumeliotis, I.; Hamilton, R. Impact of gas turbine flexibility improvements on combined cycle gas turbine performance. *Appl. Therm. Eng.* **2021**, *189*, 116703. [CrossRef]
32. Akroot, A.; Namli, L. Performance assessment of an electrolyte-supported and anode-supported planar solid oxide fuel cells hybrid system. *J. Ther. Eng.* **2021**, *7*, 1921–1935.
33. ABejan GTsatsaronis, M.M. *Thermal Design and Optimization*; John Wiley Sons Inc.: New York, NY, USA, 1996; Volume 21. [CrossRef]
34. Elmorsy, L.; Morosuk, T.; Tsatsaronis, G. Exergy-based analysis and optimization of an integrated solar combined-cycle power plant. *Entropy* **2020**, *22*, 655. [CrossRef] [PubMed]
35. Ahmadi, G.; Jahangiri, A.; Toghraie, D. Design of heat recovery steam generator (HRSG) and selection of gas turbine based on energy, exergy, exergoeconomic, and exergo-environmental prospects. *Process Saf. Environ. Prot.* **2023**, *172*, 353–368. [CrossRef]
36. Talal, W.; Akroot, A. Exergoeconomic Analysis of an Integrated Solar Combined Cycle in the Al-Qayara Power Plant in Iraq. *Processes* **2023**, *11*, 656. [CrossRef]
37. Nourpour, M.; Khoshgoftar Manesh, M.H. Evaluation of novel integrated combined cycle based on gas turbine-SOFC-geothermal-steam and organic Rankine cycles for gas turbo compressor station. *Energy Convers. Manag.* **2022**, *252*, 115050. [CrossRef]
38. Ozcan, H.; Kayabasi, E. Thermodynamic and economic analysis of a synthetic fuel production plant via CO2 hydrogenation using waste heat from an iron-steel facility. *Energy Convers. Manag.* **2021**, *236*, 114074. [CrossRef]
39. Mohammadkhani, F.; Shokati, N.; Mahmoudi, S.M.S.; Yari, M.; Rosen, M.A. Exergoeconomic assessment and parametric study of a Gas Turbine-Modular Helium Reactor combined with two Organic Rankine Cycles. *Energy* **2014**, *65*, 533–543. [CrossRef]
40. Kareem, A.F.; Akroot, A.; Abdul Wahhab, H.A.; Talal, W.; Ghazal, R.M.; Alfaris, A. Exergo–Economic and Parametric Analysis of Waste Heat Recovery from Taji Gas Turbines Power Plant Using Rankine Cycle and Organic Rankine Cycle. *Sustainability* **2023**, *15*, 9376. [CrossRef]
41. Elsafi, A.M. Exergy and exergoeconomic analysis of sustainable direct steam generation solar power plants. *Energy Convers. Manag.* **2015**, *103*, 338–347. [CrossRef]
42. Miao, X.; Zhang, H.; Zhao, S.; Zhang, Q.; Xia, Y. An innovative S–CO2 recompression Brayton system and its thermodynamic, exergoeconomic and multi-objective analyses for a nuclear spacecraft. *Case Stud. Therm. Eng.* **2024**, *53*, 103805. [CrossRef]
43. Besevli, B.; Kayabasi, E.; Akroot, A.; Talal, W.; Alfaris, A.; Assaf, Y.H.; Nawaf, M.Y.; Bdaiwi, M.; Khudhur, J. Technoeconomic Analysis of Oxygen-Supported Combined Systems for Recovering Waste Heat in an Iron-Steel Facility. *Appl. Sci.* **2024**, *14*, 2563. [CrossRef]
44. Alsunousi, M.; Kayabasi, E. Techno-economic assessment of a floating photovoltaic power plant assisted methanol production by hydrogenation of $CO_2$ captured from Zawiya oil refinery. *Int. J. Hydrog. Energy* **2024**, *57*, 589–600. [CrossRef]
45. Akroot, A.; Al Shammre, A.S. Techno-Economic and Environmental Impact Analysis of a 50 MW Solar-Powered Rankine Cycle System. *Processes* **2024**, *12*, 1059. [CrossRef]
46. Abdelhay, A.O.; Fath, H.E.S.; Nada, S.A. Case Studies in Thermal Engineering Enviro-exergo-economic analysis and optimization of a nanofiltration-multi effect desalination, power generation and cooling in an innovative trigeneration plant. *Case Stud. Therm. Eng.* **2022**, *31*, 101857. [CrossRef]
47. Tian, H.; Li, R.; Salah, B.; Thinh, P.H. Bi-objective optimization and environmental assessment of SOFC-based cogeneration system: Performance evaluation with various organic fluids. *Process Saf. Environ. Prot.* **2023**, *178*, 311–330. [CrossRef]
48. Akroot, A.; Almaktar, M.; Alasali, F. The Integration of Renewable Energy into a Fossil Fuel Power Generation System in Oil-Producing Countries: A Case Study of an Integrated Solar Combined Cycle at the Sarir Power Plant. *Sustainability* **2024**, *16*, 4820. [CrossRef]
49. Nondy, J.; Gogoi, T.K. 4E analyses of an intercooled-recuperative gas turbine-based CCHP system: Parametric analysis and tri-objective optimization. *Therm. Sci. Eng. Prog.* **2023**, *39*, 101719. [CrossRef]